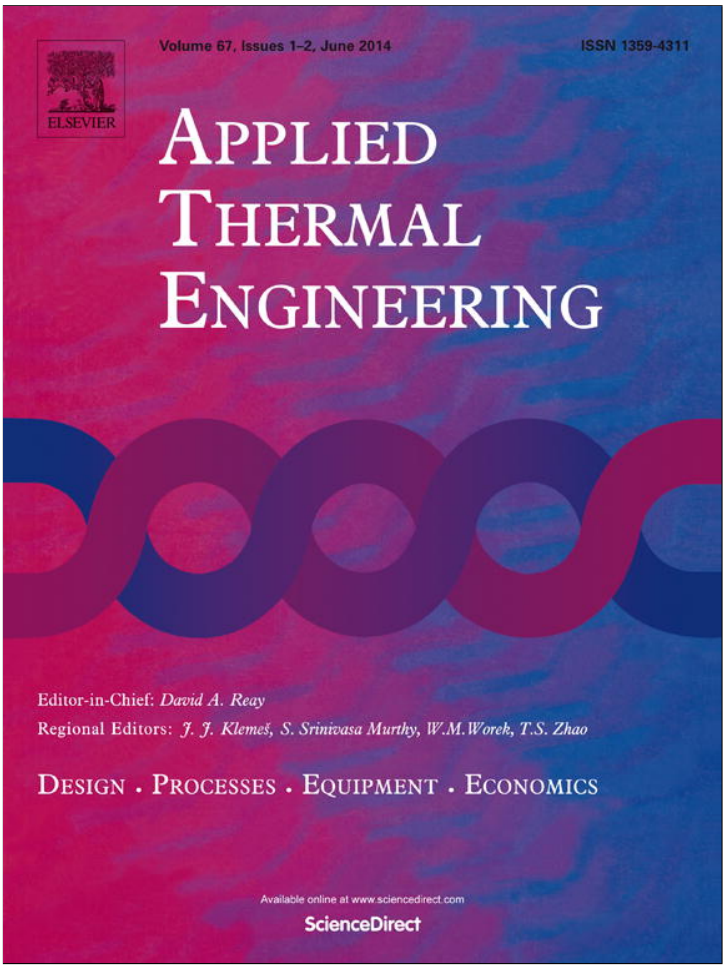

Applied Thermal Engineering 67 (2014) 439–446

Contents lists available at ScienceDirect

Applied Thermal Engineering

journal homepage: www.elsevier.com/locate/apthermeng

First-order thermal model of commercial EDLCs

Anna d'Entremont, Laurent Pilon*

University of California, Los Angeles, Henry Samueli School of Engineering and Applied Science, Mechanical and Aerospace Engineering Department, 420 Westwood Plaza, Los Angeles, CA 90095, USA

HIGHLIGHTS

- A first-order engineering model for temperature of commercial EDLCs was developed.
- Both irreversible and reversible heat generation were accounted for.
- The temperature was governed by three dimensionless similarity parameters.
- The model predictions agreed well with temperature measurements from the literature.

ARTICLE INFO

Article history:
Received 24 January 2014
Accepted 23 March 2014
Available online 4 April 2014

Keywords:
Supercapacitors
Energy storage
Joule heating
Scaling analysis

ABSTRACT

This study presents a first-order thermal analysis for electric double layer capacitors (EDLCs). It is based on the lumped-capacitance approximation and accounts for both irreversible and reversible internal heat generation. A simple analytical expression for the overall temperature rise during galvanostatic cycling was derived. A scaling analysis was performed and demonstrated with experimental data collected from commercial EDLCs. This thermal model enables rapid estimation of reversible heat generation and prediction of the temperature evolution in EDLCs without performing computationally intensive numerical simulations.

1. Introduction

Electric double layer capacitors (EDLCs) physically store electric charge within the electric double layer (EDL) forming at the mesoporous electrode/electrolyte interface. They are promising electrical energy storage devices filling the gap between batteries and conventional dielectric capacitors [1,2]. EDLCs offer significantly larger power densities, longer cycle life, and higher cycle efficiencies than batteries, while still offering higher energy densities than conventional capacitors [1–5].

During operation, heat is generated within EDLCs, resulting in temperature rise in the device [2–6]. The heat generation rate and temperature changes depend on the design, materials, and operating conditions of the cell [3]. Elevated temperatures have detrimental effects on EDLCs including (i) accelerated ageing [2–7], (ii) increased self-discharge rates [2,4–6], and (iii) increased cell pressure [6]. Thermal modeling can be used to predict EDLC operating temperatures and develop thermal management strategies to avoid these harmful effects.

The present study aims to develop a first-order thermal model and the associated scaling analysis to predict the general thermal behavior of EDLC devices. Scaling analysis has been widely used in physics and engineering analyses of complex systems. It reduces the number of independent parameters to be considered in the analysis and facilitates the development of widely-applicable thermal design rules [8]. Model predictions were compared with experimental measurements on commercial EDLCs reported in the literature [4,5].

2. Background

2.1. Experimentally observed thermal behavior of EDLCs

Experimental studies have investigated the thermal behavior of commercial EDLCs [3–6,9] and lab-built EDLC cells [10,11] subjected to galvanostatic cycling under current $\pm I_s$. They observed an overall temperature rise from cycle to cycle proportional to I_s^2 and attributed to irreversible Joule heating [3–6,9–11]. In addition,

* Corresponding author.
E-mail address: pilon@seas.ucla.edu (L. Pilon).

http://dx.doi.org/10.1016/j.applthermaleng.2014.03.061
1359-4311/

Nomenclature

A	external surface area (m^2)
C	capacitance (F)
C_{th}	heat capacity (J/K)
e	elementary charge (C)
$\overline{h}$	average convective heat transfer coefficient (W/m^2 K)
I_s	electric current (A)
k_B	Boltzmann constant (J/K)
n_c	number of charge/discharge cycles
$\dot{Q}$	heat generation rate (W)
R	electrical resistance (Ω)
R_{th}	thermal resistance (K/W)
T	temperature (K)
T_0	initial temperature (K)
T_∞	ambient temperature (K)
t	time (s)
t_c	cycle period (s)
V_0	volume of electrolyte (m^3)
V_S	volume of Stern layer (m^3)

Greek symbols

α	semi-empirical parameter characterizing reversible heating (V)
τ^*_{th}	dimensionless thermal time constant
$\Delta\psi$	electric potential window (V)
ψ_s	voltage across EDLC (V)

Superscripts and subscripts

*	refers to dimensionless variable
irr	refers to irreversible heat generation
rev	refers to reversible heat generation

superimposed temperature oscillations at the same frequency as the charge–discharge cycles were observed and attributed to reversible heating [4,9–11]. The reversible heat generation rate was empirically found to be exothermic during charging, endothermic during discharging, and proportional to the current I_s [4,11].

2.2. Thermal models of EDLCs

Previous EDLC thermal models typically predicted the temperature of the device by solving the transient heat diffusion equation in one [12], two [5,9], or three dimensions [10,13,14]. Guillemet et al. [2] solved the two-dimensional steady-state heat diffusion equation to predict the steady-state local temperature and ignored temperature oscillations due to reversible heat generation. Chiang et al. [15] predicted the temporal temperature evolution of an EDLC accounting for reversible heat generation but neglecting spatial temperature variations. Other studies have employed the electric circuit analogy [2,6,7]. Most of these studies treated EDLCs as "black boxes" characterized experimentally to retrieve parameters necessary for the thermal models [2,5–7,13,14]. The heat generation rate was prescribed as either (i) uniform throughout the entire device [5,6,9,10,15], (ii) uniform in the "active components," i.e., the electrodes and separator [13,14], or (iii) as having different values in the current collectors, electrodes, and separator [2]. The irreversible heat generation rate was either imposed as an input parameter [2,5,10,13] or predicted as Joule heating (in W) equal to $I_s^2 R$, where R was the experimentally measured resistance of the EDLC cell [4,6,7,14,15].

Most existing thermal models ignored reversible heat generation and typically did not consider in detail the electrochemical phenomena occurring inside the device [2,5,6,10,13,14]. However, Schiffer et al. [4] developed an expression for the reversible heat generation rate $\dot{Q}_{rev}$ based on estimated changes in the entropy of the ions due to electric double layer formation. Their derivation approximated the EDL as a monolayer of ions and assumed that the capacitance was independent of the cell potential. The reversible heat generation rate (in W) was expressed as [4]

$$\dot{Q}_{rev} = -2\frac{Tk_B}{e}\ln\left(\frac{V_S}{V_0}\right)C\frac{d\psi_s}{dt} = -2\frac{Tk_B}{e}\ln\left(\frac{V_S}{V_0}\right)I_s(t) \quad (1)$$

where T is the temperature, k_B is the Boltzmann constant, and e is the elementary charge. The cell capacitance, cell voltage, and current were denoted by C, ψ_s, and I_s, respectively. The total electrolyte volume and the Stern layer volume were given by V_S and V_0. However, the value of V_S/V_0 is difficult to evaluate for porous electrodes. Instead, it is often used as a fitting parameter. Nonetheless, the expression of $\dot{Q}_{rev}$ given by Equation (1) was later adopted by other thermal models [7,9,15].

In a recent study [12], we derived a local thermal model from first principles, elucidating the origin of reversible heat generation and predicting both the local irreversible and reversible volumetric heat generation rates within binary and symmetric electrolytes. The model was solved for coupled electric potential, ion concentrations, and temperature during galvanostatic cycling of a thermally insulated cell with planar electrodes. Predictions of temperature evolution under various conditions showed remarkable qualitative resemblance to experimental data [4,9,12]. Although entropy changes contributed to reversible heating, the expression for $\dot{Q}_{rev}$ suggested by Equation (1) was found to be inconsistent with that predicted by first principles [12].

Predicting the temperature field in actual EDLC devices using our model [12] would require significant computing resources given the complexity of actual porous electrode architectures. Instead, developing a simple engineering thermal model for actual EDLCs would provide a simplified alternative and a convenient engineering tool to rapidly predict the thermal behavior of EDLCs. Scaling analysis can further simplify the analysis to obtain thermal design rules for actual devices. In this study, a lumped-capacitance model of EDLCs subjected to galvanostatic cycling was developed accounting for both irreversible and reversible internal heating.

3. Analysis

The following assumptions were made: (1) the device properties were constant, (2) the thermal resistance to heat transfer between the EDLC and its surroundings was constant, and (3) temperature gradients within the device were small compared to that between the EDLC and its surroundings, so that lumped-capacitance analysis was appropriate. In fact, for large cycling currents, the measured temperature difference between the outer surface of commercial devices and their surroundings was significantly larger than the temperature difference inside the device [5,6].

3.1. Dimensional energy balance

Thermal energy balance performed on the entire EDLC device yields the governing equation for its temperature $T(t)$ expressed as [8]

$$C_{\text{th}}\frac{dT}{dt} = \dot{Q}(t) - \frac{[T(t) - T_\infty]}{R_{\text{th}}} \tag{2}$$

where C_{th} is the heat capacity of the device (in J/K) and $\dot{Q}(t)$ is the internal heat generation rate (in W), including both irreversible and reversible heating. The second term on the right-hand side of Equation (2) represents the rate of heat transfer (in W) from the device to its surrounding environment at temperature T_∞, characterized by the thermal resistance R_{th} (in K/W). The latter may be expressed as $R_{\text{th}} = 1/\bar{h}A$, where $\bar{h}$ is the average convective heat transfer coefficient (in W/m^2 K) and A is the external surface area of the device (in m^2).

The total heat generation rate consists of irreversible and reversible contributions, i.e., $\dot{Q}(t) = \dot{Q}_{\text{irr}}(t) + \dot{Q}_{\text{rev}}(t)$. During galvanostatic cycling, the current $I(t)$ is a square signal of magnitude I_s with cycle period t_c. Then, the irreversible heat generation rate is constant and equal to $\dot{Q}_{\text{irr}} = I_s^2 R$, where R is the electrical resistance of the EDLC [4,11,12]. As previously mentioned, the reversible heat generation rate is exothermic during charging, endothermic during discharging, and proportional to I_s [4,11,12]. Here, it is assumed to be a square wave expressed as

$$\dot{Q}_{\text{rev}}(t) = \begin{cases} +\alpha I_s & \text{during charging} \\ -\alpha I_s & \text{during discharging} \end{cases} \tag{3}$$

where α is a positive semi-empirical parameter specific to each device and expressed in V.

Finally, Equation (2) is a first-order, linear ordinary differential equation (ODE) requiring one initial condition. Here, the EDLC's initial temperature was assumed to be equal to T_0, i.e., $T(t=0) = T_0$.

3.2. Scaling analysis

The governing Equation (2) was non-dimensionalized using the dimensionless variables

$$t^* = \frac{t}{t_c} \quad \text{and} \quad T^*(t^*) = \frac{T(t) - T_0}{I_s^2 R t_c / C_{\text{th}}}. \tag{4}$$

The time t was scaled by the cycle period t_c, while the temperature change $T(t) - T_0$ was scaled by the temperature rise per cycle associated with the irreversible heating and expressed as $\dot{Q}_{\text{irr}} t_c / C_{\text{th}} = I_s^2 R t_c / C_{\text{th}}$.

Substituting Equation (4) into the energy conservation Equation (2) yields the governing equation for the dimensionless temperature $T^*(t^*)$

$$\frac{dT^*}{dt^*} = 1 - \frac{T^*(t^*) - T_\infty^*}{\tau_{\text{th}}^*} + \dot{Q}_{\text{rev}}^*(t^*). \tag{5}$$

Here, $T_\infty^* = (T_\infty - T_0)/(I_s^2 R t_c / C_{\text{th}})$ is the dimensionless ambient temperature. The dimensionless thermal time constant is defined as $\tau_{\text{th}}^* = R_{\text{th}} C_{\text{th}} / t_c$, where the thermal time constant $R_{\text{th}} C_{\text{th}}$ characterizes how rapidly the EDLC temperature responds to changes in its thermal environment [8]. Finally, the dimensionless heat generation rate $\dot{Q}_{\text{rev}}^* = \dot{Q}_{\text{rev}}/\dot{Q}_{\text{irr}} = \pm\alpha/I_s R$ represents the ratio of the reversible to the irreversible heat generation rates. The initial condition is expressed in dimensionless form as $T^*(0) = 0$.

The dimensionless ODE given by Equation (5) can be solved to yield the following expression for the dimensionless temperature

$$T^*(t^*) = (\tau_{\text{th}}^* + T_\infty^*)\left(1 - e^{-t^*/\tau_{\text{th}}^*}\right) + e^{-t^*/\tau_{\text{th}}^*} \int_0^{t^*} e^{t^{*\prime}/\tau_{\text{th}}^*} \dot{Q}_{\text{rev}}^*(t^{*\prime}) dt^{*\prime}. \tag{6}$$

3.3. Irreversible and reversible temperatures

Based on the superposition principle, the temperature $T(t)$ may be viewed as the sum of two contributions associated with irreversible and reversible heat generation so that $T(t) = T_{\text{irr}}(t) + T_{\text{rev}}(t)$. The overall temperature $T_{\text{irr}}(t)$, resulting from $\dot{Q}_{\text{irr}}$, accounts for the temperature rise from cycle to cycle, while the reversible temperature oscillations $T_{\text{rev}}(t)$ result from $\dot{Q}_{\text{rev}}$. These contributions can be expressed in dimensionless form as

$$T_{\text{irr}}^*(t^*) = \frac{T_{\text{irr}}(t) - T_0}{I_s^2 R t_c / C_{\text{th}}} \quad \text{and} \quad T_{\text{rev}}^*(t^*) = \frac{T_{\text{rev}}(t)}{I_s^2 R t_c / C_{\text{th}}}. \tag{7}$$

For an EDLC cooled by convection, T_{irr}^* is expressed as

$$T_{\text{irr}}^*(t^*) = (\tau_{\text{th}}^* + T_\infty^*)\left(1 - e^{-t^*/\tau_{\text{th}}^*}\right) \tag{8}$$

and is governed by two dimensionless similarity parameters, namely, τ_{th}^* and T_∞^*. Over time, T_{irr}^* approaches a steady-state value given by $T_{\text{irr}}^*(t^* \to \infty) = \tau_{\text{th}}^* + T_\infty^*$. In dimensional form, $T_{\text{irr}}(t)$ can be written as

$$T_{\text{irr}}(t) = T_0 + \left(I_s^2 R R_{\text{th}} + T_\infty - T_0\right)\left(1 - e^{-t/R_{\text{th}}C_{\text{th}}}\right). \tag{9}$$

Thus, under steady-state conditions, the irreversible temperature is expressed as $T_{\text{irr}}(t \to \infty) = R_{\text{th}} I_s^2 R + T_\infty$. Subtracting Equation (8) from Equation (6) yields

$$T_{\text{rev}}^*(t^*) = e^{-t^*/\tau_{\text{th}}^*} \int_0^{t^*} e^{t^{*\prime}/\tau_{\text{th}}^*} \dot{Q}_{\text{rev}}^*(t^{*\prime}) dt^{*\prime}. \tag{10}$$

3.4. Perfectly insulated EDLC

In the limiting case of a perfectly thermally insulated EDLC, R_{th} and τ_{th}^* approach infinity. Then, $\tau_{\text{th}}^* \gg t^*$ and $e^{-t^*/\tau_{\text{th}}^*} \approx 1 - t^*/\tau_{\text{th}}^*$, so that the overall dimensionless temperature rise is linear with t^* and given in dimensionless and dimensional form by

$$T_{\text{irr}}^*(t^*) = t^* \quad \text{and} \quad T_{\text{irr}}(t) = T_0 + \frac{I_s^2 R}{C_{\text{th}}} t. \tag{11}$$

Similarly, the dimensionless reversible temperature can be expressed as

$$T_{\text{rev}}^*(t^*) = \begin{cases} \pm\left|\dot{Q}_{\text{rev}}^*\right|(t^* - n_c) & 0 \le (t^* - n_c) < 1/2 \\ \pm\left|\dot{Q}_{\text{rev}}^*\right|[(n_c + 1) - t^*] & 1/2 \le (t^* - n_c) < 1 \end{cases} \tag{12}$$

where $n_c = 0, 1, 2\ldots$ is the number of completed charge–discharge cycles. Here, the positive and negative signs correspond to cycling starting with a charging or a discharging step, respectively. In dimensional form, $T_{\text{rev}}(t)$ can be expressed as

$$T_{\text{rev}}(t) = \begin{cases} \pm\dfrac{\alpha I_s}{C_{\text{th}}}(t - n_c t_c) & n_c t_c \le t < (n_c + 1/2) t_c \\ \pm\dfrac{\alpha I_s}{C_{\text{th}}}[(n_c + 1) t_c - t] & (n_c + 1/2) t_c \le t < (n_c + 1) t_c. \end{cases} \tag{13}$$

3.5. Method of solution

The dimensionless temperature $T^*(t^*)$ accounting for reversible heat generation was evaluated by numerically solving Equation (5)

using an explicit third-order Runge–Kutta method [16]. The solver adjusted the time step to satisfy specified relative and absolute tolerances. It compared the estimated error associated with $T^*(t^*)$ to these tolerances at each time step. The convergence criterion was defined such that the relative error in the dimensionless temperature T^* was less than 0.5% when dividing both tolerances by two.

3.6. Experimental data

Table 1 summarizes the values of the capacitance C, electrical resistance R, heat capacity C_{th}, and thermal resistance R_{th} of commercial EDLCs whose thermal behaviors have been investigated in the literature [4–6] including Maxwell BCAP1500 [17], Maxwell BCAP0350 [18], and Nesscap ESHCP-5000C0-002R7 [19]. Note that C_{th} for the Nesscap 5000 F cell was measured experimentally and reported in Ref. [4]. The Maxwell EDLCs were cooled by natural convection in air at T_∞ [5,6] while the Nesscap cell was thermally insulated [4]. Table 1 also provides the operating conditions including the current I_s, potential window $\Delta\psi$, initial temperature T_0, and ambient air temperature T_∞, used in three experimental studies reported in the literature [4–6]. The cycle period t_c was estimated from the device capacitance C, the potential window $\Delta\psi$, and the current I_s according to $t_c = 2C\Delta\psi/I_s$ [4]. Experimental data from these different studies were used to validate the present model and the associated scaling analysis.

4. Results and discussion

4.1. Parametric study

Fig. 1(a) shows $T^*(t^*)$ predicted by solving Equation (5) and $T^*_{irr}(t^*)$ predicted by Equation (8) as functions of t^* for τ^*_{th} ranging from 10 to ∞ with $T^*_\infty = 0$. The cycles started with a charging step and $\left|\dot{Q}^*_{rev}\right|$ was equal to 5. In all cases, the temperature $T^*(t^*)$ featured nearly triangular temperature oscillations around T^*_{irr}, as predicted by Equation (12) in the limiting case of τ^*_{th} approaching infinity. For finite values of τ^*_{th}, T^*_{irr} initially satisfied $T^*_{irr}(t^* \approx 0) \approx t^*$, and T^*_{irr} approached the steady-state value $T^*_{irr}(t^* \to \infty) = T^*_\infty + \tau^*_{th}$ as convective heat losses increased due to the increasing temperature difference between the device and the surroundings. In other words, in the oscillatory steady-state regime, the rate of heat loss to the surroundings balances the irreversible heat generation rate.

Table 1
Properties of commercial EDLC devices and galvanostatic cycling conditions used in experimental studies [4–6]. The experimental data were used to demonstrate the present analysis and scaling.

Manufacturer	Units	Maxwell Tech. [17]	Maxwell Tech. [18]	Nesscap Co. [19]
		BCAP1500	BCAP0350	ESHCP-5000C0-002R7
C	(F)	1500	350	5000
R	(mΩ)	0.47	3.2	0.33
C_{th}	(J/K)	320	60	1118 [4]
R_{th}	(K/W)	3.2	10.9	∞ [4]
α	(V)	0.04–0.07	0.1–0.2	0.06
Exp. studies		Al Sakka et al. [6]	Gualous et al. [5]	Schiffer et al. [4]
I_s	(A)	75	30	25–100
$\Delta\psi$	(V)	1.35	1.25	1–2
$t_c = 2C\Delta\psi/I_s$	(s)	54	29	100–400
T_0	(°C)	17.5	20	25
T_∞	(°C)	17.5	20	
Dimensionless similarity parameters				
τ^*_{th}		19.0	22.4	∞
T^*_∞		0	0	–
$T^*(t^* \to \infty)$		19.0	22.4	∞

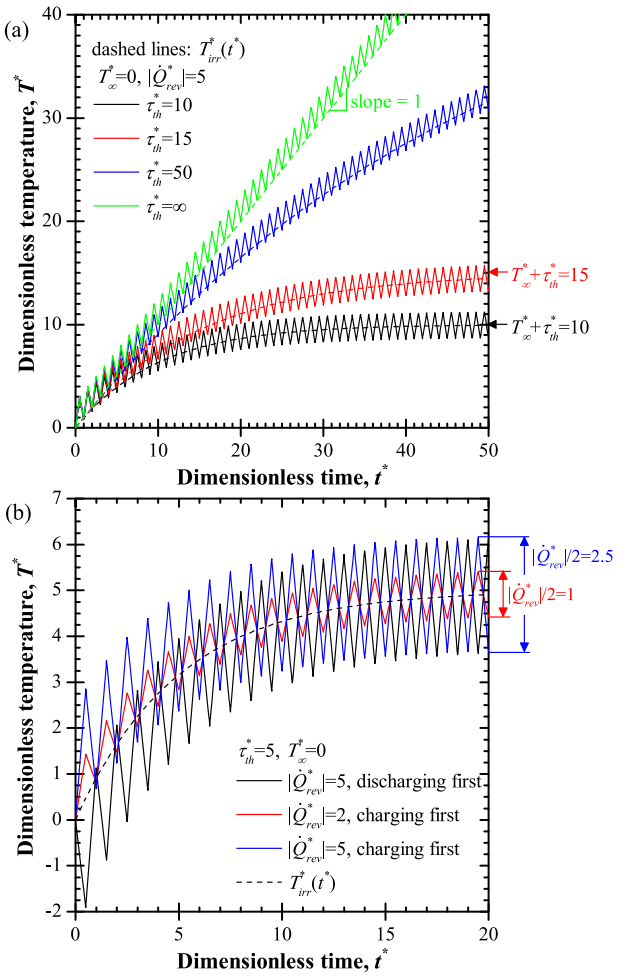

Fig. 1. Dimensionless temperature $T^*(t^*)$ predicted by solving Equation (5) and dimensionless irreversible temperature $T^*_{irr}(t^*)$ given by Equation (8) as functions of t^* for (a) different values of τ^*_{th} with $T^*_\infty = 0$ for $\left|\dot{Q}^*_{rev}\right| = 5$ and (b) different values of $\left|\dot{Q}^*_{rev}\right|$ for $T^*_\infty = 0$ and $\tau^*_{th} = 5$..

This relationship could be used in practice to determine the values of τ^*_{th} and $R_{th} = t_c\tau^*_{th}/C_{th}$ of actual EDLCs.

Similarly, Fig. 1(b) shows $T^*(t^*)$ predicted by solving Equation (5) and $T^*_{irr}(t^*)$ given by Equation (8) as functions of t^* for $\tau^*_{th} = 5$ and $T^*_\infty = 0$. Here, $\left|\dot{Q}^*_{rev}\right|$ was equal to either 2 or 5 and the cycle started with either a discharging or a charging step. The local maxima and minima of $T^*(t^*)$ occurred at the end of the charging steps and of the discharging steps, respectively. In cases beginning with a charging step, $T^*(t^*)$ initially increased and oscillated within the envelope $T^*_{irr}(t^*) \le T^*(t^*) \le T^*_{irr}(t^*) + \left|\dot{Q}^*_{rev}\right|/2$ where $T^*_{irr}(t^*)$ is given by Equation (8). By contrast, in cases beginning with a discharging step, $T^*(t^*)$ initially decreased, oscillating within the range $T^*_{irr}(t^*) \ge T^*(t^*) \ge T^*_{irr}(t^*) - \left|\dot{Q}^*_{rev}\right|/2$. However, as $T^*(t^*)$ approached oscillatory steady-state, all cases fell within the envelope $T^*_{irr}(t^*) - \left|\dot{Q}^*_{rev}\right|/4 \le T^*(t^*) \le T^*_{irr}(t^*) + \left|\dot{Q}^*_{rev}\right|/4$. Interestingly, the amplitude of the dimensionless temperature oscillations ΔT^*_{rev} was equal to $\left|\dot{Q}^*_{rev}\right|/2 = \alpha/2I_sR$ at all times and for all cases considered, as illustrated in Fig. 1(b). In dimensional form, it is expressed as $\Delta T_{rev} = \alpha I_s t_c/2C_{th}$. In fact, this provides a simple and convenient way to estimate the coefficient of proportionality α associated with reversible heat generation directly from experimental data as $\alpha = 2C_{th}\Delta T_{rev}/I_s t_c$.

4.2. EDLCs cooled by natural convection

Fig. 2 shows the temperatures $T(t)$ as a function of time t measured by Gualous and coworkers at the outer surface of (a) a 1500 F EDLC [6] and (b) a 350 F EDLC [5] galvanostatically cycled at ±75 A and ±30 A, respectively. These Maxwell Technologies EDLCs were cooled by natural convection in air at T_∞ of 20 and 17.5 °C, respectively [5,6]. Both figures display a clear overall temperature rise with small temperature oscillations. Here also, the temperature rose quickly at the beginning of the test and then approached an oscillatory steady-state as the rate of convective heat loss balanced the irreversible heat generation rate. Fig. 2(a) and (b) also plot T_{irr} predicted by Equation (9) using properties summarized in Table 1 as well as predictions for thermal resistance $R_{\text{th}} \pm 10\%$ to account for the possible uncertainty in the reported values of R_{th}. In both Fig. 2(a) and (b), experimental data fell approximately between the temperature predictions of Equation (9) using $R_{\text{th}} \pm 10\%$.

Fig. 2(c) and (d) plot the data shown in Fig. 2(a) and (b) in terms of dimensionless temperature $T^*(t^*)$ and time t^*. They also show the overall dimensionless temperature rise $T^*_{\text{irr}}(t^*)$ predicted by Equation (8). Here also, predictions for $T^*_{\text{irr}}(t^*)$ were in good agreement with scaled temperature measurements for both EDLCs. In addition, the dimensionless temperature oscillations were small compared to the overall dimensionless temperature rise, i.e., $\dot{Q}^*_{\text{rev}}/2$ was small compared to $\tau^*_{\text{th}} + T^*_\infty$. It was difficult to accurately quantify the temperature oscillation amplitude ΔT_{rev} in order to retrieve α. However, from visual inspection, ΔT^*_{rev} ranged approximately between 1/2 and 1 for both EDLCs, yielding α between 0.04 V and 0.07 V for BCAP1500 and 0.1 V and 0.2 V for BCAP0350. This corresponded to a dimensional temperature oscillation amplitude ΔT_{rev} between 0.2 K and 0.4 K for BCAP1500 and between 0.7 K and 1.4 K for BCAP0350.

4.3. Thermally insulated EDLC

Fig. 3(a) shows the temperature $T(t)$ measured at the surface of a thermally insulated 5000 F EDLC (ESHCP-5000C0-002R7 by Nesscap Co.) as a function of time t. This EDLC was cycled galvanostatically at currents I_s between 25 and 100 A and cycle periods t_c ranging from 100 to 400 s [4]. The electrical resistance R, the heat capacity C_{th}, the thermal resistance R_{th}, and the ambient temperature T_∞ remained the same for all five cases and are summarized in Table 1. The temperature featured oscillations superimposed over an approximately linear temperature rise of slope $I_s^2 R$ [4].

Fig. 3(b) shows the same data as in Fig. 3(a) but in dimensionless form. The scaled data for all five cases approximately collapsed around an overall temperature rise predicted by $T^*_{\text{irr}} = t^*$ and corresponding to the limiting case when τ^*_{th} or R_{th} approached infinity.

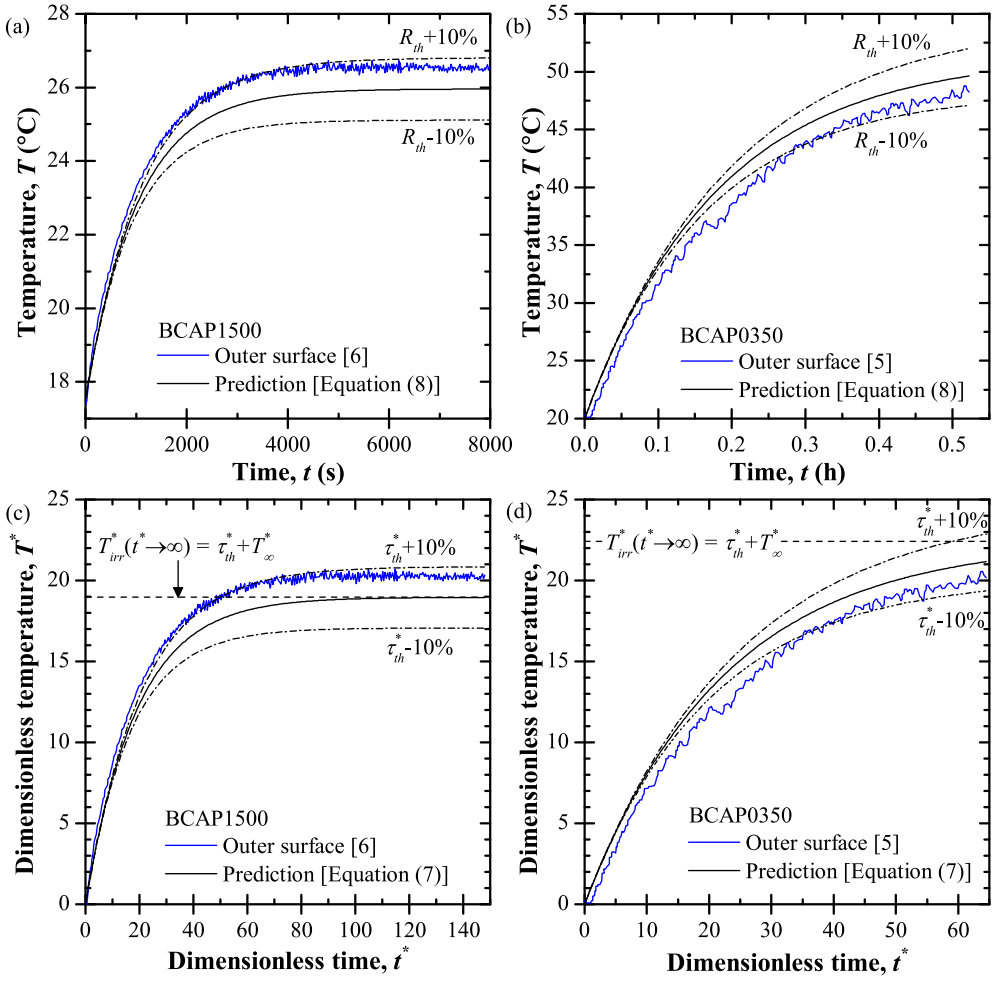

Fig. 2. Measured temperature $T(t)$ as a function of time t at the outer surface of (a) a 1500 F EDLC cycled at ±75 A (Fig. 7 of Ref. [6]) and (b) a 350 F EDLC cycled at ±30 A (Fig. 8 of Ref. [5]), as well as (c) and (d) the corresponding dimensionless temperatures $T^*(t^*)$ as functions of dimensionless time t^* and the predictions by Equation (8) using data in Table 1.

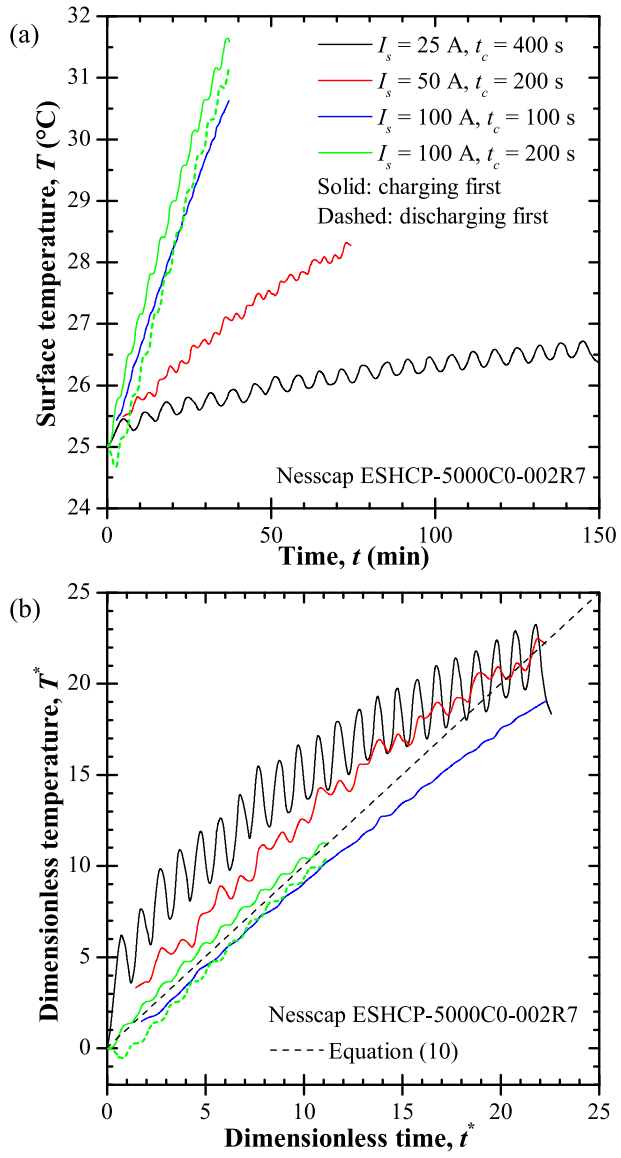

Fig. 3. (a) Measured temperature $T(t)$ at the surface of a thermally insulated Nesscap 5000 F EDLC as a function of time t for different values of current I_s and cycle period t_c (Figs. 8 and 10 of Ref. [4]) and (b) the corresponding dimensionless temperature $T^*(t^*)$ as well as $T^*_{irr}(t^*)$ predicted by Equation (11) as functions of dimensionless time t^*.

As observed in Fig. 1, the initial slope dT^*_{irr}/dt^* in the experimental data was equal to about 1. However, as T^* increased, the overall slope of the measured T^* slowly decreased. This can be attributed to heat losses to the surroundings due to imperfect thermal insulation. In fact, R_{th} and τ^*_{th} were large but finite, and $T^*(t^*)$ would eventually approach an oscillatory steady-state around the dimensionless temperature $T^*_{irr}(t^* \to \infty) = \tau^*_{th} + T^*_\infty$ similar to the behavior shown in Fig. 1. This behavior was more apparent at smaller currents when irreversible heat generation was smaller. For larger current I_s, heat generation was large compared with convective heat losses to the surroundings in the time frame for which data are available. Unfortunately, the steady-state EDLC temperature could not be evaluated because the actual values of R_{th} and τ^*_{th} were not measured. It is also interesting to note that, by scaling t by the cycle period t_c, the temperature maxima and minima occurred at the same dimensionless times t^*.

Fig. 4 plots the same data as in Fig. 3(a) separately in terms of dimensionless temperature $T^*(t^*)$ as a function of t^* for cycles beginning with a charging step with (a) $I_s = 25$ A, (b) $I_s = 50$ A, and (c) $I_s = 100$ A as well as (d) a case beginning with a discharging step with $I_s = 100$ A. It also plots the predictions for $T^*(t^*)$ obtained by numerically solving Equation (5). As previously discussed, the dimensionless temperature oscillation amplitude was equal to $\Delta T^*_{rev} = \left|\dot{Q}^*_{rev}\right|/2 = \alpha/2I_sR$. These oscillations were the largest for experimental data with $I_s = 25$ A [Fig. 4(a)]. Thus, the average value of ΔT^*_{rev} was estimated for this dataset to yield the semi-empirical constant $\alpha = 2\Delta T^*_{rev} I_s R = 0.06 \pm 0.012$ V with 95% confidence interval. This value of α was of the same order of magnitude as those estimated for the other EDLCs. In addition, it was the same for all datasets considered in Fig. 4, since they were collected with the same device. The corresponding values of $\left|\dot{Q}^*_{rev}\right|$ ranged from 1.8 to 7.3 as the current I_s decreased from 100 A to 25 A. This explained why the temperature oscillations shown in Fig. 4 were significantly larger than those observed in Fig. 2, when $\left|\dot{Q}^*_{rev}\right|$ was estimated to range between 1 and 2. The larger values of $\left|\dot{Q}^*_{rev}\right|$ in the Nesscap EDLC were likely due to (i) smaller cycling currents and/or (ii) smaller resistance R (Table 1).

Overall, predictions of $T^*(t^*)$ closely resembled the measured behavior. However, there was a temporal offset between the predicted and measured temperature oscillations. In fact, Fig. 4 indicates that the local maxima and minima of the measured T^* were shifted towards later dimensionless times t^* compared with predictions obtained by solving Equation (9). This effect was also observed in our previous first-principles modeling study [12]. The delay was attributed to heat diffusion from the electrode/electrolyte interface to the bulk electrolyte [12]. Indeed, reversible heat generation occurs mainly near the electrode surface where the electric double layer forms and is transported by conduction through the electrolyte and electrode to the outer surface of the EDLCs.

Moreover, the measured $T^*(t^*)$ was larger than the model predictions for cases beginning with a charging step [Fig. 4(a) and (b)] and smaller for cases beginning with a discharging step [Fig. 4(d)]. This can also be attributed to heat diffusion inside the EDLC. In fact, our previous study [12] showed that the temperature oscillation amplitude decreases with increasing distance from the electric double layer. Thus, retrieving the reversible heat generation rate and the parameter α from surface temperature measurements underpredicted its actual value since temperature oscillations were larger inside the device.

Finally, the present model predicts the main features of the experimental data quite well. Fig. 5 summarizes the procedure to predict the overall temperature rise $T_{irr}(t)$ and the temperature oscillation amplitude ΔT_{rev}. It provides an excellent first-order estimate of the EDLC temperature behavior without relying on detailed and computationally intensive numerical simulations. In addition, it offers a simple and convenient method for retrieving the thermal resistance R_{th} and the semi-empirical parameter α for reversible heat generation from experimental temperature measurements. Note that α is the only empirical parameter retrieved from temperature measurements. All the other input parameters can be obtained from product data sheets. In addition, the model's irreversible temperature predictions agreed well with experimental measurements reported in the literature for EDLCs of different sizes and manufacturers. This suggests that the present model is robust and broadly applicable.

5. Conclusion

This study developed an engineering thermal model accounting for both irreversible and reversible heat generation to predict the

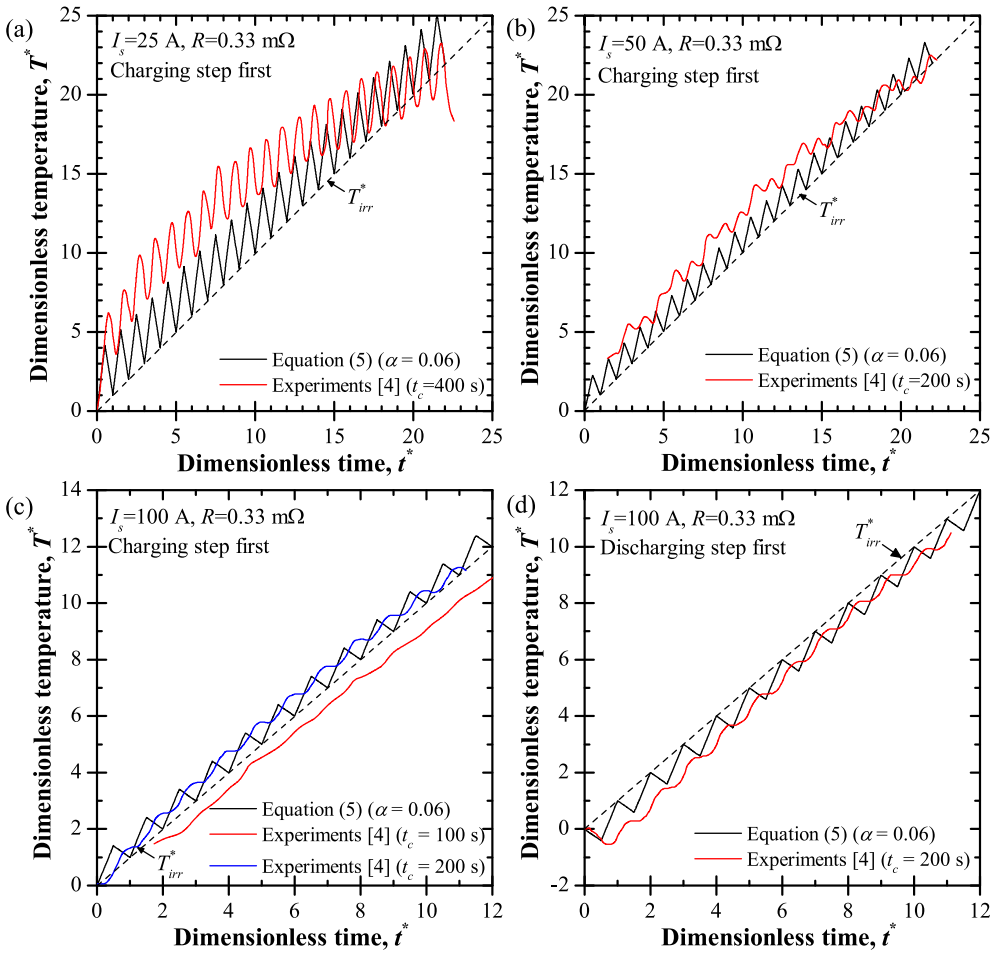

Fig. 4. Dimensionless temperature $T^*(t^*)$ as a function of dimensionless time t^* based on experimental measurements at the EDLC outer surface [4] and predicted by solving Equation (5) for a thermally insulated EDLC cycled at (a) $I_s = 25$ A, (b) $I_s = 50$ A, and (c) $I_s = 100$ A beginning with a charging step as well as (d) cycled at $I_s = 100$ A beginning with a discharging step.

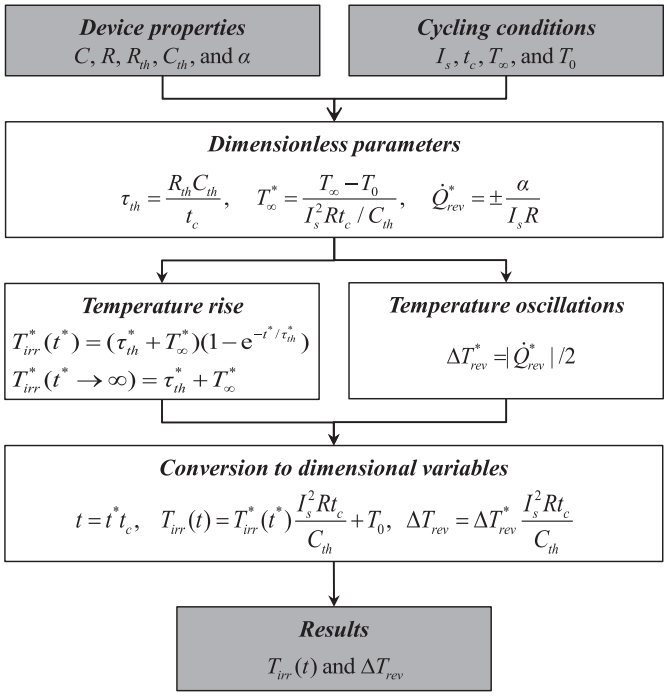

Fig. 5. Procedure to estimate temperature evolution of an EDLC.

temporal evolution of temperature in EDLC devices during galvanostatic cycling. The dimensionless temperature $T^*(t^*)$ was governed by three dimensionless similarity parameters, namely, τ^*_{th}, T^*_∞, and $\dot{Q}^*_{rev}$, characterizing the rate of heat transfer to the surroundings, the ambient temperature, and the reversible heat generation rate, respectively. Temperature predictions showed good agreement with experimental data obtained from different commercial devices and reported in the literature [4–6]. This first-order model has the advantage of predicting the temperature evolution of actual EDLC devices without relying on computationally intensive numerical simulations. It can be used in designing thermal management strategies for EDLCs.

Acknowledgements

This material is based upon work supported by the National Science Foundation Graduate Research Fellowship under Grant No. DGE-1144087 and as part of the Molecularly Engineered Energy Materials, an Energy Frontier Research Center funded by the U.S. Department of Energy, Office of Science, Office of Basic Energy Sciences under Award Number DE-SC0001342.

References

[1] US Department of Energy, Basic Research Needs for Electrical Energy Storage: Report of the Basic Energy Sciences Workshop for Electrical Energy Storage, Tech. rep., Office of Basic Energy Sciences, DOE, 2007. URL: http://www.osti.gov/accomplishments/documents/fullText/ACC0330.pdf

[2] P. Guillemet, Y. Scudeller, T. Brousse, Multi-level reduced-order thermal modeling of electrochemical capacitors, J. Power Sources 157 (1) (2006) 630–640.
[3] J.R. Miller, Electrochemical capacitor thermal management issues at high-rate cycling, Electrochim. Acta 52 (4) (2006) 1703–1708.
[4] J. Schiffer, D. Linzen, D.U. Sauer, Heat generation in double layer capacitors, J. Power Sources 160 (1) (2006) 765–772.
[5] H. Gualous, H. Louahlia-Gualous, R. Gallay, A. Miraoui, Supercapacitor thermal modeling and characterization in transient state for industrial applications, IEEE Trans. Ind. Appl. 45 (3) (2009) 1035–1044.
[6] M. Al Sakka, H. Gualous, J. Van Mierlo, H. Culcu, Thermal modeling and heat management of supercapacitor modules for vehicle applications, J. Power Sources 194 (2) (2009) 581–587.
[7] O. Bohlen, J. Kowal, D.U. Sauer, Ageing behaviour of electrochemical double layer capacitors: part II. Lifetime simulation model for dynamic applications, J. Power Sources 173 (1) (2007) 626–632.
[8] F.P. Incropera, D.P. DeWitt, T.L. Bergman, A.S. Lavine, Fundamentals of Heat and Mass Transfer, sixth ed., John Wiley & Sons, Hoboken, NJ, 2007.
[9] H. Gualous, H. Louahlia, R. Gallay, Supercapacitor characterization and thermal modelling with reversible and irreversible heat effect, IEEE Trans. Power Electron. 26 (11) (2011) 3402–3409.
[10] C. Pascot, Y. Dandeville, Y. Scudeller, P. Guillemet, T. Brousse, Calorimetric measurement of the heat generated by a double-layer capacitor cell under cycling, Thermochim. Acta 510 (2010) 53–60.
[11] Y. Dandeville, P. Guillemet, Y. Scudeller, O. Crosnier, L. Athouel, T. Brousse, Measuring time-dependent heat profiles of aqueous electrochemical capacitors under cycling, Thermochim. Acta 526 (2011) 1–8.
[12] A.L. d'Entremont, L. Pilon, First-principles thermal modeling of electric double layer capacitors under constant-current cycling, J. Power Sources 246 (2014) 887–898.
[13] D.H. Lee, U.S. Kim, C.B. Shin, B.H. Lee, B.W. Kim, Y.-H. Kim, Modelling of the thermal behaviour of an ultracapacitor for a 42-V automotive electrical system, J. Power Sources 175 (1) (2008) 664–668.
[14] K. Wang, L. Zhang, B. Ji, J. Yuan, The thermal analysis on the stackable supercapacitor, Energy 59 (0) (2013) 440–444.
[15] C.-J. Chiang, J.-L. Yang, W.-C. Cheng, Temperature and state-of-charge estimation in ultracapacitors based on extended Kalman filter, J. Power Sources 234 (2013) 234–243.
[16] P. Bogacki, L.F. Shampine, A 3(2)pair of Runge–Kutta formulas, Appl. Math. Lett. 2 (1989) 321–325.
[17] Datasheet: K2 Series Ultracapacitors, Product Data Sheet 1015370.3, Maxwell Technologies, Inc., San Diego, CA.
[18] Datasheet: BC Series Ultracapacitors, Product Data Sheet 1017105.3, Maxwell Technologies, Inc., San Diego, CA.
[19] Nesscap Ultracapacitor Products, Product Specification Sheet: Large, Prismatic Ultracapacitors, Nesscap Co., Ltd., South Korea, 2008. URL: http://www.nesscap.com.